^{11}C-DPA-713: A Novel Peripheral Benzodiazepine Receptor PET Ligand for In Vivo Imaging of Neuroinflammation

Hervé Boutin[1–3], Fabien Chauveau[1,2], Cyrille Thominiaux[1], Marie-Claude Grégoire[4,5], Michelle L. James[5], Régine Trebossen[1], Philippe Hantraye[4], Frédéric Dollé[1], Bertrand Tavitian[1,2], and Michael Kassiou[7–9]

[1]CEA, Institut d'Imagerie Biomédicale, Service hospitalier Frédéric Joliot, Laboratoire d'Imagerie Moléculaire Expérimentale, Orsay, France; [2]INSERM, U803, Orsay, France; [3]Faculty of Life Sciences, Neurobiology Group, University of Manchester, Manchester, United Kingdom; [4]CNRS URA 2210, CEA, DSV, 12BM, SHFJ, Orsay, France; [5]RRI, ANSTO, Menai, Australia; [6]Department of Pharmacology, University of Sydney, Sydney, New South Wales, Australia; [7]School of Medical Radiation Sciences, University of Sydney, Sydney, New South Wales, Australia; [8]School of Chemistry, University of Sydney, Sydney, New South Wales, Australia; and [9]Ramaciotti Centre for Brain Imaging, Brain and Mind Research Institute, University of Sydney, Sydney, New South Wales, Australia

The induction of neuroinflammatory processes, characterized by upregulation of the peripheral benzodiazepine receptor (PBR) expressed by microglial cells, is well correlated with neurodegenerative diseases and with acute neuronal loss. The continually increasing incidence of neurodegenerative diseases in developed countries has become a major health problem, for which the development of diagnostic and follow-up tools is required. Here we investigated a new PBR ligand suitable for PET to monitor neuroinflammatory processes as an indirect hallmark of neurodegeneration. **Methods:** We compared PK11195, the reference compound for PBR binding sites, with the new ligand DPA-713 (*N*,*N*-diethyl-2-[2-(4-methoxyphenyl)-5,7-dimethylpyrazolo[1,5-*a*]pyrimidin-3-yl]acetamide), using a small-animal dedicated PET camera in a model of neuroinflammation in rats. Seven days after intrastriatal injection of α-amino-3-hydroxy-5-methyl-4-isoxazolepropionate (AMPA), a PET scan was performed using ^{11}C-PK11195 or ^{11}C-DPA-713. Immunohistochemistry for neuronal (NeuN), astrocyte (glial fibrillary acidic protein), and microglial (CD11) specific markers as well as ^{3}H-PK11195 autoradiographic studies were then correlated with the imaging data. **Results:** Seven days after a unilateral injection of AMPA in the striatum, ^{11}C-DPA-713 exhibits a better contrast between healthy and damaged brain parenchyma than ^{11}C-PK11195 (2.5-fold ± 0.14 increase vs. 1.6-fold ± 0.05 increase, respectively). ^{11}C-DPA-713 and ^{11}C-PK11195 exhibit similar brain uptake in the ipsilateral side, whereas, in the contralateral side, ^{11}C-DPA-713 uptake was significantly lower than ^{11}C-PK11195. Modeling of the data using the simplified reference tissue model shows that the binding potential was significantly higher for ^{11}C-DPA-713 than for ^{11}C-PK11195. **Conclusion:** ^{11}C-DPA-713 displays a higher signal-to-noise ratio than ^{11}C-PK11195 because of a lower level of unspecific binding that is likely related to the lower lipophilicity of ^{11}C-DPA-713. Although further studies in humans are required, ^{11}C-DPA-713 represents a suitable alternative to ^{11}C-PK11195 for PET of PBR as a tracer of neuroinflammatory processes induced by neuronal stress.

Key Words: PET; inflammation; gliosis; peripheral benzodiazepine receptor; PK11195

J Nucl Med 2007; 48:573–581
DOI: 10.2967/jnumed.106.036764

Over the past decades, the incidence of neurodegenerative disease in the elderly population of developed countries has increased considerably (*1,2*). This has led to an increased research effort from the academic and the pharmaceutical industry in the development of new therapies for treating diseases such as Alzheimer's, Parkinson's, or Huntington's disease. There is now a wealth of evidence that suggests an active participation of glial mechanisms in deciding the fate of injured nerve cells: either causing cell death by the release of cytotoxic metabolites or enabling recovery through provision of growth or survival factors (*3,4*). Genomic and transcriptomic data show that many brain diseases—irrespective of their classification as neurodegenerative, inflammatory, or neoplastic—call into action similar sets of genes and associated pathways. Prominent among these sets of genes are those traditionally associated with inflammation or, in the case of brain diseases, "neuroinflammation" (*4,5*). On histologic postmortem investigation, neurodegenerative disorders reveal pronounced changes in the functional state of glial cells with activation of both microglial cells and astrocytes (*6–9*). The microglial activation process is associated with an increase in the number of microglial cells and the expression of numerous proteins (*3–5*). The peripheral benzodiazepine receptor (PBR), one of these newly expressed proteins, is considered a reliable marker of microglial activation and neuroinflammation and, therefore, an important therapeutic and diagnostic target (*10–12*).

Received Sep. 26, 2006; revision accepted Jan. 20, 2007.
For correspondence or reprints contact: Bertrand Tavitian, MD, Laboratoire d'Imagerie Moléculaire Expérimentale, 4 place du général Leclerc, F-91400 Orsay, France.
E-mail: bertrand.tavitian@cea.fr

The noninvasive imaging technique of PET is the method of choice for the study in living subjects of biochemical processes such as receptor–ligand interactions, allowing translation of research from animal models to humans. The prototypical PBR ligand PK11195 has been radiolabeled with the short-lived PET isotope ^{11}C (half-life = 20.3 min). This radioligand has been used to image active brain pathology in several conditions, including stroke, multiple sclerosis, encephalitis, Parkinson's disease, and Alzheimer's disease (*8,10,13–16*). This has provided the proof-of-principle that the estimation of PBR expression in vivo and the measurement of microglial activation in neurodegenerative brain is possible (*8,17*). However, the high degree of nonspecific uptake of ^{11}C-PK11195 complicates the quantification and modeling of the PET data (*18–21*). This significantly limits its sensitivity in detecting brain injury and, importantly, may not adequately detect the subtle changes in PBR expression affected by therapeutic intervention.

The development of new PBR ligands with higher specific binding would provide a major advance to the imaging of neuroinflammation and strengthen its value as a diagnostic index, especially if the detection of subtle or diffuse changes in PBR expression is required. Consequently, the aim of the present work was the in vivo validation of the recently reported PBR radioligand ^{11}C-DPA-713 (*22,23*) in a model of neurodegeneration—namely, the excitotoxic lesion of the striatum in rats.

MATERIALS AND METHODS

Animal Surgery

All studies were conducted in accordance with French legislation and European directives. Wistar rats (average body weight, 299 ± 50 g [mean ± SD]; Centre d'Élevage René Janvier, France) were kept in thermoregulated, humidity-controlled facilities under a 12-h light/12-h dark cycle (light on between 7 h AM and 7 h PM) and were allowed free access to food and water. Anesthesia was induced by 5% isoflurane and thereafter maintained by 2%–2.5% in a 70%:30% mixture of NO_2/O_2. α-Amino-3-hydroxy-5-methyl-4-isoxazolepropionate ([AMPA] 15 mM in phosphate-buffered saline [PBS] buffer; Sigma) was stereotactically injected through the use of a 1-μL microsyringe and micropump (injection rate, 0.5 μL/min; UltraMicroPump II and Micro4 Controller; WPI Inc.). AMPA (0.5 μL) was injected in the right striatum (Bregma +0.7 mm, from sagittal suture: 2.7 mm; depth from brain surface: 5.5 mm). Animals were maintained normothermic (body temperature, 36.7°C ± 0.5°C; mean ± SD) during the surgery through the use of a heating blanket (Homeothermic Blanket Control Unit; Harvard Apparatus Ltd.).

Histologic Study

Because no contrast between healthy and damaged brain tissue was observed in sections stained with cresyl violet 7 d after inducing the striatal lesion—mainly due to glial cells invading the lesion site—the volume of the brain damage was assessed 2 d postlesion in 7 Wistar rats (body weight, 300 ± 68 g; mean ± SD). Brains were quickly removed and frozen in isopentane in dry ice. Brain damage, delineated by the relative paleness of histologic staining in the damaged tissue, was assessed on cresyl violet–stained coronal sections (20 μm). According to the methods described by Osborne et al. (*24*), ipsilateral healthy tissue, contralateral hemisphere, and lesion volumes were calculated by the integration of areas as quantified with a computer-assisted image analyzer on each brain slice. Lesion volumes were computed using SigmaScan Pro software (Systat Software, Inc.).

Immunohistochemical Study

Immunohistochemistry staining was also performed on 7 rats (body weight, 295 ± 58 g; mean ± SD) immediately after the end of the PET scans. Animals were euthanized and brains were quickly removed and frozen in isopentane in dry ice. Two adjacent sets of rat brain sections were fixed in paraformaldehyde (4% in 100 mM PBS) for 1 h and washed (6 × 5 min) in PBS. Sections were permeabilized with 30 min of incubation in 0.1% Triton X-100 containing 4.5% normal goat serum in PBS to block nonspecific binding. Without further washing, sections were incubated overnight at 4°C with primary antibodies in 3% normal goat serum/0.1% Triton X-100 in PBS. At each level, 1 section was stained for both glial fibrillary acidic protein (GFAP) with rabbit anticow GFAP (DakoCytomation, 1:1,000) and CD11b (Ox42) with mouse antirat CD11b (Serotec, 1:1,000), and 1 for both GFAP and NeuN (mouse antimouse NeuN, 1:1,000; Chemicon). Sections were then washed (3 × 10 min) in PBS and incubated for 1 h at room temperature with secondary antibodies (Alexa Fluor 594-nm goat antimouse IgG, Alexa Fluor 488-nm goat antirabbit IgG, both 1:500; Molecular Probes, Invitrogen) in 3% normal goat serum/0.1% Triton X-100 in PBS and then washed again (3 × 10 min) in PBS.

Sections were mounted with a Prolong Antifade kit (Molecular Probes, Invitrogen); those incubated without the primary antibodies served as negative controls.

Fluorescent examination was performed on an Olympus AX70 microscope equipped with a DP50 charged-coupled device camera. Magnifications used were 4×, 10×, and 20× (Universal Plan Apochromat objectives), and images were acquired with analySIS software (Soft Imaging System).

Autoradiography

Concomitantly with the first ^{11}C-PK11195 PET scans performed and before proceeding further, the presence of specific PBR binding sites in the lesion was confirmed by autoradiographic experiments with ^{3}H-PK11195 (Amersham) on rat brain sections 2 d (n = 6), 3 d (n = 2), and 7 d (n = 2) after AMPA injection (rat body weight, 286 ± 61 g; mean ± SD). ^{3}H-PK11195 was used at a concentration of 18 nM in Tris buffer (based on its affinity for the PBR; 50 mM, pH 7.4, at 4°C) according to protocols described elsewhere (*17*). Nonspecific binding was determined by incubation of adjacent brain slices in the presence of 10 μM Ro5-4864 (Sigma). Brain sections were exposed for 3 h in a β-imager (Biospace Mesures) using β-Acquisition control and acquisition software (Biospace Mesures). Subsequent analysis of acquired images was performed using β-Vision+ software (Biospace Mesures).

Radiosynthesis of Ligands

(*R*)-PK11195 ((R)-*N*-Methyl-*N*-(1-methylpropyl)-1-(2-chlorophenyl)isoquinoline-3-carboxamide) was labeled with ^{11}C at its amide moiety from the corresponding *nor*-derivative ((*R*)-*N*-(1-methylpropyl)-1-(2-chlorophenyl)isoquinoline-3-carboxamide) using ^{11}C-methyl iodide (*25,26*) (Both *nor*-(*R*)-PK11195 and PK11195 were kindly provided by Sanofi-Aventis). Typically, about 4.80 GBq of (*R*)-^{11}C-PK11195 (>98% radiochemically pure)

were routinely obtained within 25 min of radiosynthesis (including high-performance liquid chromatography [HPLC] purification and formulation), with specific radioactivities ranging from 75 to 90 GBq/μmol. DPA-713 (*N*,*N*-diethyl-2-[2-(4-methoxyphenyl)-5,7-dimethylpyrazolo[1,5-*a*]pyrimidin-3-yl]acetamide) was labeled with ^{11}C at its aromatic methoxy moiety from the corresponding *nor*-derivative (*N*,*N*-diethyl-2-[2-(4-hydroxyphenyl)-5,7-dimethylpyrazolo[1,5-*a*]pyrimidin-3-yl]acetamide) using ^{11}C-methyl triflate (*22*,*23*) (DPA-713 and *nor*-DPA-713 were synthesized according to James et al. (*22*)). Typically, about 7.40 GBq of ^{11}C-DPA-713 (>98% radiochemically pure) were routinely obtained within 20 min of radiosynthesis (including HPLC purification and formulation), with specific radioactivities ranging from 70 to 90 GBq/μmol.

PET Scans and Data Acquisition

On the basis of the autoradiographic results, 17 rats were used for imaging 7 d after AMPA injection and distributed among groups as follows (body weight expressed as mean ± SD): ^{11}C-PK11195, 275 ± 50 g, $n = 5$; ^{11}C-DPA-713, 300 ± 10 g, $n = 4$; ^{11}C-DPA-713 + PK11195, 306 ± 7 g, $n = 4$; ^{11}C-DPA-713 + DPA-713, 345 ± 38 g, $n = 4$. Anesthesia was induced by 5% isoflurane and thereafter maintained by 2%–2.5% isoflurane in a 70%:30% mixture of NO_2/O_2. For PET scans, the rat's head was placed in a home-made stereotactic frame compatible with PET acquisition, and rats were maintained normothermic (rectal temperature, 36.7°C ± 0.5°C; mean ± SD) through the use of a heating blanket (Homeothermic Blanket Control Unit; Harvard Apparatus Ltd.). Seven days after intrastriatal injection of AMPA, expression of PBR was assessed through the use of a Focus 220 PET scanner (Siemens Medical Solutions USA, Inc.) using either ^{11}C-PK11195 or ^{11}C-DPA713. Radiolabeled compounds (^{11}C-PK11195, 72.2–110 MBq, 1.88–23.7nmol; ^{11}C-DPA-713, 61.1–90.74 MBq, 0.67–2.07nmol) and unlabeled ligands (1 mg/kg) were injected in the caudal vein through a 24-gauge catheter. Radiolabeled compounds were injected concomitantly with the start of PET acquisition and unlabeled compounds were injected 20 min after injection of radiotracers. PET data were acquired for 80 min.

The acquisition protocol consisted of the following parameters: The time coincidence window was set to 6 ns, and the levels of energy discrimination were set to 350 and 750 keV. The list-mode acquisition data files were histogrammed into 3-dimensional sinograms with a maximum ring difference of 47 and a span of 3. The list-mode data of the emission scans were sorted into 14 dynamic frames. The attenuation correction factors were measured using an external ^{68}Ge point source. Finally, the emission sinograms (each frame) were normalized, corrected for attenuation and radioactivity decay, and reconstructed using Fourier rebinning and 2-dimensional ordered-subsets expectation maximization (16 subsets and 4 iterations).

Image Analysis

PET image analysis was performed using ASIPro VM (Analysis Tools and System Setup/Diagnostics Tool; Siemens Medical Solutions USA, Inc.). Regions of interest (ROIs) were delineated as contralateral and ipsilateral hemisphere, cerebellum, and lesion (as delineated by the hyper-signal seen in the summed image of the 14 frames); the mirror ROI of the lesion was copied and symmetrically pasted into the contralateral hemisphere. In the case of overlapping of the 2 ROIs due to a thalamic lesion, the contralateral ROI was reduced to the edge of the ipsilateral ROI.

PET Data Modeling

The simplified reference tissue model (*27*) from the PMOD software package (PMOD Technologies Ltd., version 2.5) was used to assess the binding potential (BP) in rat brain structures. This model relies on a 2-tissue reversible compartment for the target region (ipsilateral ROI) and a single-tissue compartment for the reference region (contralateral ROI). The model assumes that the nonspecific compartment is either negligible or that its exchange rates with the free compartment are sufficiently rapid. In addition, the distribution volume of the free compartment (DV1) is supposed to be equal in both reference and target structures. Finally, the reference region–measured kinetics should not include any specific binding. The analysis of the double-injection kinetics, particularly after injection of unlabeled ligand, supports these assumptions. Three parameters were estimated for each kinetic: R1 (k_1/k'_1), which represents the ratio of tracer delivery; k_2, which is the clearance from the target tissue back to the vascular compartment; and the BP (k_3/k_4).

Metabolite Analysis in Rat Blood and Brain

Naive or adult male Wistar rats that underwent surgery (body weight, 300–400 g) were injected intravenously in the tail vein with ^{11}C-DPA-713 (88–158 MBq). Animals were sacrificed 10, 20, or 30 min later. A blood sample was collected, and plasma was isolated by centrifugation (5 min, 3,000 rpm). Plasma proteins were precipitated from 400 μL of serum by addition of 400 μL of CH_3CN. After centrifugation (5 min, 3,000 rpm), the supernatant was injected onto the HPLC column. Rat brains were removed and hemispheres were separated. Homogenization by sonication was performed in 1 mL of acetonitrile per hemisphere. After a rapid centrifugation, the supernatant was separated from the pellet and concentrated under reduced pressure before injection onto the HPLC column (HPLC equipment: model 600 Controller [Waters], 1100 Series UV detector [Hewlett Packard], Flow One Scintillation detector [Packard]; column: semipreparative C18, μBondapak column [Waters], 300 × 7.8 mm; porosity: 10 μm; solvent A: 0.1% aqueous trifluoroacetic acid (TFA); solvent B: CH_3CN, isocratic elution: 60:40 (A/B) in 10 min; flow rate: 6 mL/min; room temperature; absorbance detection at $\lambda = 263$ nm).

Blood–Brain Barrier (BBB) Integrity

The integrity of the BBB was investigated using Evans blue extravasation. Evans blue (2% in saline, 4 mL/kg) was injected intravenously in control animals or at 1, 2, or 7 d postlesion. After decapitation, brains were quickly removed and frozen in isopentane in dry ice, digital pictures of the brain were taken during cryostat sectioning and in 50-μm sections, and Evans blue extravasation was compared between groups.

Statistical Analysis

All data are expressed as mean ± SD. All comparisons were performed using Kruskal–Wallis and Mann–Whitney nonparametric tests. For all statistical analyses, the significance level accepted was $P < 0.05$.

RESULTS

Histologic and Immunohistochemical Studies

Injection of 7.5 nmol of AMPA in the right striatum induced a lesion of reproducible size and shape in the striatum 48 h after injection (21.0 ± 5.7 mm^3) (Fig. 1). Six rats were examined 48 h after intrastriatal injection, showing that the lesion was strictly limited to the striatum in 3 animals, and brain damage had extended into the thalamus in 3 of 6 animals (Fig. 1). Cortical damage (excluding the needle track) was observed in 1 of 6 rats and located in the piriform cortex. Using fast cresyl violet staining, the lesion was clearly identifiable at 48 h after injection (Fig. 1), but the contrast between healthy tissue and lesion site faded at longer postlesion times, and the delineation of the lesion was barely identifiable at 7 d after injection. Therefore, immunohistochemistry was preferred to histology to measure brain damage: Astroglial and microglial invasion was clearly observed using specific antibodies (Figs. 2 and 3). The location of brain damage was similar at 48 h and 7 d after injection (neuronal loss and induction of glial cells in the striatum in all animals, in the piriform cortex in 29% of the rats, and in the thalamus in 57% of the rats).

BBB Integrity

We observed Evans blue staining in the striatum and in the cortex at the needle track level at 1 or 2 d after inducing the lesion; however, at 7 d after injection, a slight Evans blue extravasation was observed in only 1 of 7 rats (data not shown).

PET

Seven days postlesion, the use of ^{11}C-PK11195 to image PBR expression correlated well with induction of microglial cells observed using immunohistochemistry or PBR expression using ^{3}H-PK11195 autoradiography (Figs. 2–4). As shown by the pharmacokinetics of ^{11}C-PK11195 (Fig. 5A), the first peak was within the first minute after injection; this was followed by a slow decrease in the ipsilateral ROI and a slightly more rapid washout in the contralateral ROI during the 10 min after injection. Thereafter, the pharmacokinetics of ^{11}C-PK11195 were parallel in both ipsilateral and contralateral sides. Quantification of PET data highlighted a significant difference between the contralateral and ipsilateral sides (1.6-fold ± 0.05 increase in the percentage injected dose per cubic centimeter (%ID/cm^3 in the ipsilateral side when compared with the contralateral side, between 10 and 70 min). Lower specific radioactivity for 2 of the 5 ^{11}C-PK11195 PET experiments (data not shown) did not affect significantly the time–activity curves or the contrast between the ipsilateral and contralateral side or the BP values, suggesting that all experiments were performed at tracer doses. Similarly, the use of fixed-size ROIs around the center of the lesion highlights similar results with ROIs including the whole lesion (data not shown).

For ^{11}C-DPA-713, the pharmacokinetics in the brain was slightly different than that for ^{11}C-PK11195: ^{11}C-DPA-713 did not peak as high as ^{11}C-PK11195 during the first minutes after injection but rather quickly reached a plateau and then decreased slowly with time. As shown in Figure 5B, the brain concentration of ^{11}C-DPA-173 was significantly different between ipsilateral and contralateral sides (2.5-fold ± 0.14 increase in %ID/cm^3 in ipsilateral side when compared with contralateral side, between 10 and 70 min).

Only intact radioligand was detected in the brain 10, 20, and 30 min after injection of ^{11}C-DPA-713 (retention time, 7.3 min). Two metabolites, more hydrophilic than ^{11}C-DPA-713, were detected in the plasma 10 and 30 min after injection (intact form of ^{11}C-DPA-713, 73% and 57%–66% at 10 and 30 min after injection, respectively; $n = 2$ per time point; metabolite's retention time, 2.1 and 3.0 min). No lipophilic compounds were eluted after the intact radioligand despite the wash of the HPLC column (water + 0.1% TFA:acetonitrile 20:80; 10 min).

Comparison of the pharmacokinetics of ^{11}C-PK11195 and ^{11}C-DPA-713 highlighted that uptake of both ligands was not significantly different in the lesion site but that the uptake of ^{11}C-DPA-713 was significantly lower than the uptake of ^{11}C-PK11195 in healthy tissue (Fig. 5C). A first trial of PET data modeling was performed to estimate the BP of both ^{11}C-PK11195 and ^{11}C-DPA-713 in the rat brain. R_1 values ($= k_1/k'_1$) were close to unity for ^{11}C-PK11195 (^{11}C-PK11195 = 1.10 ± 0.05) and slightly above 1 for ^{11}C-DPA-713 (R_1 = 1.32 ± 0.16). BP was significantly higher for ^{11}C-DPA-713 than that for ^{11}C-PK11195 (1.57 ± 0.36

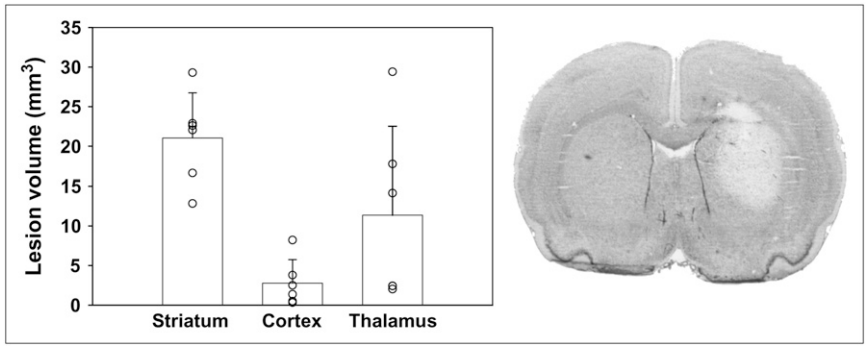

FIGURE 1. After 2 d, quantification of lesion volumes (left) highlights a reproducible lesion volume in ipsilateral striatum. In cortical areas, lesion size was more variable and essentially due to the needle track, except in 1 rat, and in thalamic nuclei, in which lesion had extended for 3 of 6 rats. Lesion was clearly delineated on coronal section (20 μm) with cresyl violet staining in ipsilateral striatum after AMPA injection (right) (×4).

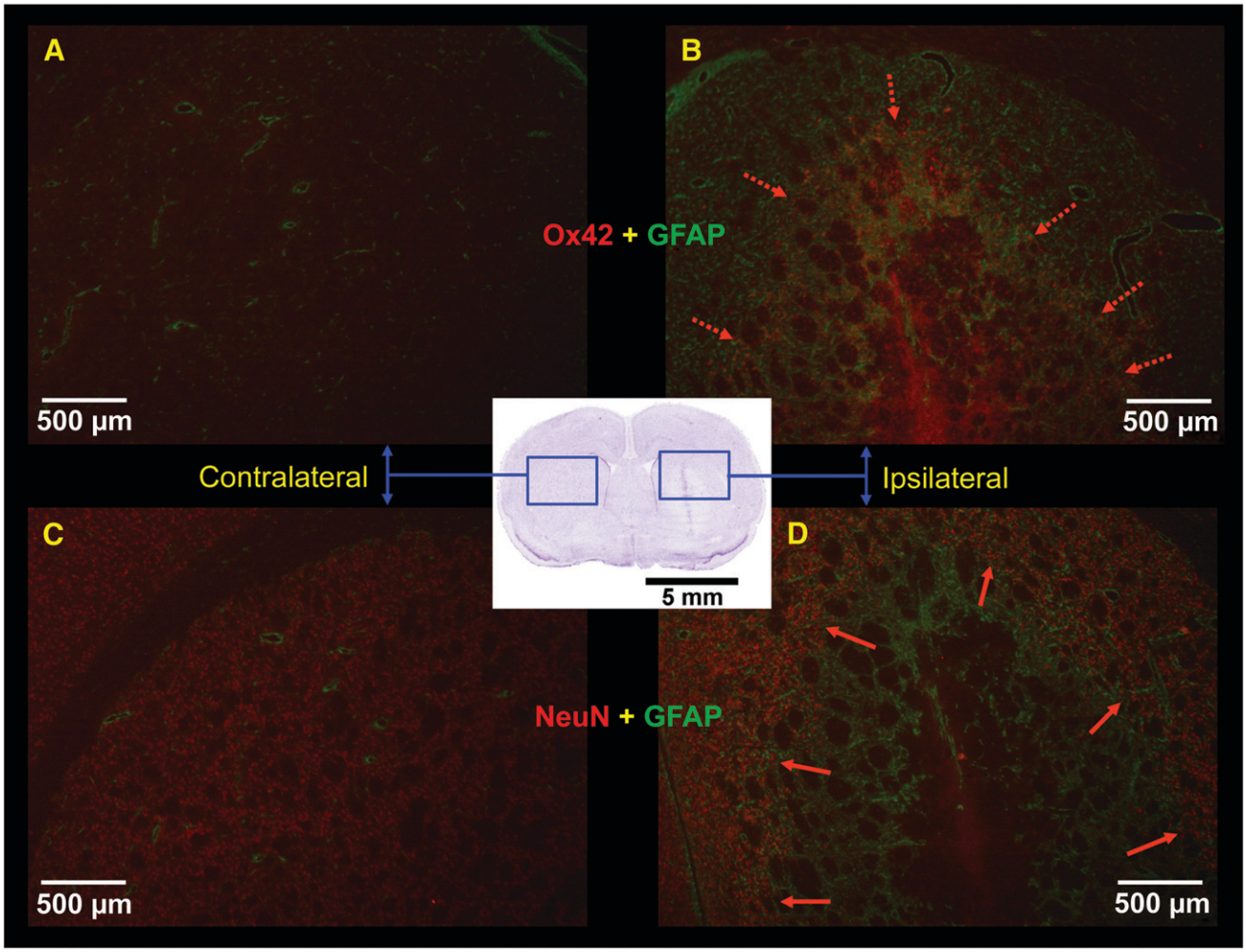

FIGURE 2. Immunohistochemistry was performed 7 d after intrastriatal injection on 2 adjacent sets of rat brain sections (postfixed with paraformaldehyde): 1 for GFAP (green staining) and CD11b antigen (Ox42, red staining) (A and B); the other for GFAP (green) and neuron-specific nuclear protein (NeuN, red staining) (C and D). In contralateral side (A and C), clear NeuN staining was observed, whereas no activated microglial cells or astrocytes could be seen. In ipsilateral side, intense microglial activation (red) was observed within lesion core surrounded by a clear astroglial activation (green) (delineated by dashed arrows in B), whereas neuronal loss was clearly seen in lesion core when compared with surrounding healthy tissue (delineated by solid arrows in D).

vs. 0.66 ± 0.15; $P < 0.05$, Mann–Whitney test). Because $R_1 > 1$ for ^{11}C-DPA-713, we have also simulated a new curve with $R_1 = 1$ and unchanged k_2 and BP values to evaluate the impact of a potential undetected alteration of the BBB and altered K_1. This fit showed no significant difference between the simulated curve and experimental plots from 11 ± 3 min onward.

Displacement studies were performed by injecting an excess (1 mg/kg) of either unlabeled PK11195 or DPA-713, 20 min after injection of ^{11}C-DPA-713 (Fig. 6). Before injection of unlabeled PK11195 (0–20 min), brain pharmacokinetics of ^{11}C-DPA-713 were not significantly different, when compared with the single-injection experiments, in both ipsilateral and contralateral sides, whereas the basal level of ^{11}C-DPA-713 was slightly lower before injection of unlabeled DPA-713 (0–20 min) than that in the ^{11}C-DPA-713 single injection. Rapid displacement of ^{11}C-DPA-713 in the brain was observed in the lesion site with both unlabeled PK11195 (Fig. 6A) and DPA-713 (Fig. 6B) from 20 to 80 min after injection, whereas no change in ^{11}C-DPA-713 concentration was observed in the contralateral side.

DISCUSSION

In the present study, we have used a small-animal dedicated PET scanner to investigate the new PBR radioligand ^{11}C-DPA-713 (*22,23*). Although the PBR is only modestly expressed in normal brain parenchyma, it is dramatically upregulated in neuropathologic conditions, including stroke, brain trauma, Alzheimer's disease, and Parkinson's disease, correlating with the activation of microglial cells. We first performed a microPET study using the known PBR radioligand ^{11}C-PK11195 in rats with a striatal lesion. The localization and expression of PBR correlate well with the results obtained ex vivo (Figs. 2–4). Similarly, clinical studies have

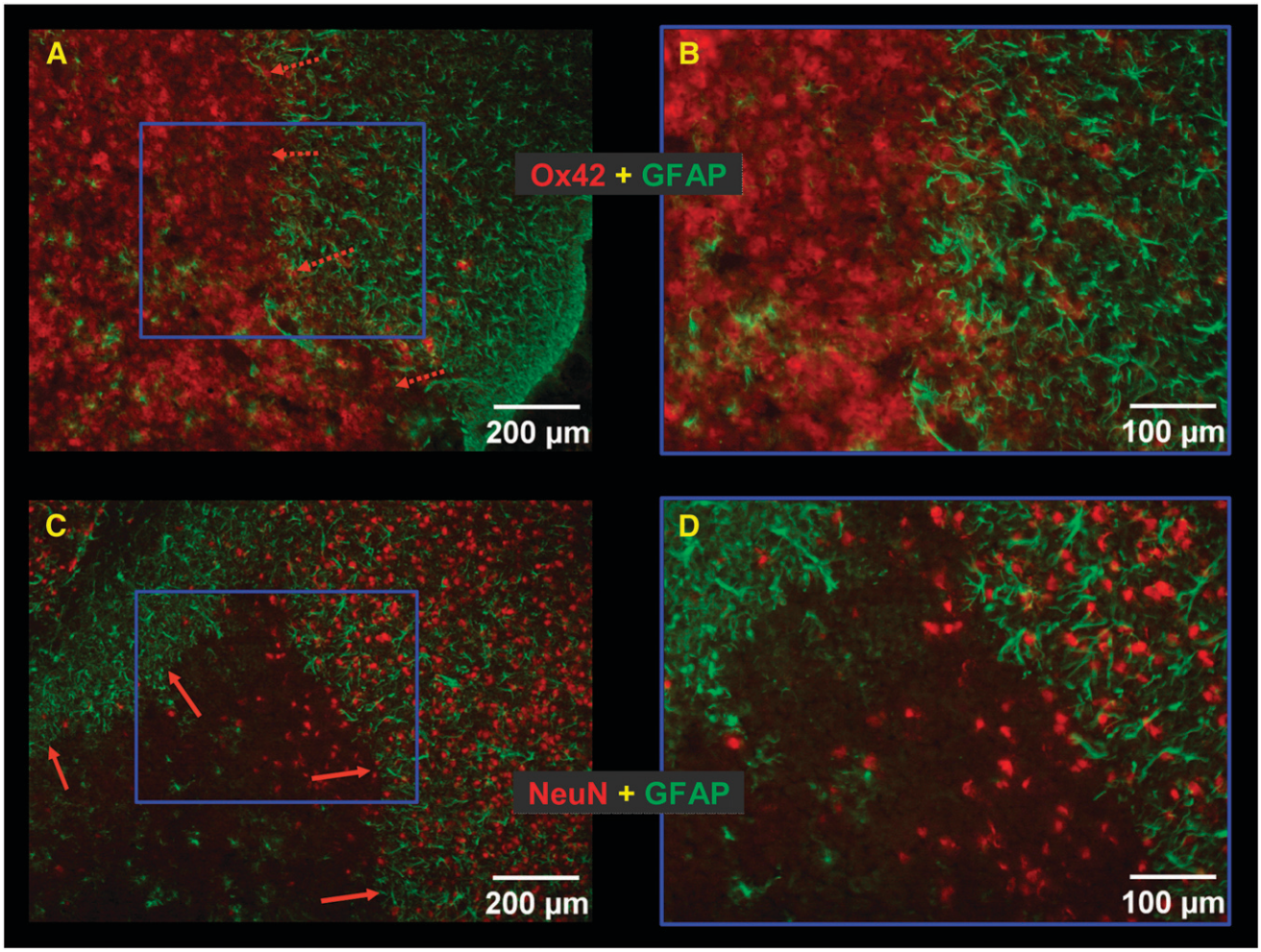

FIGURE 3. High magnification of immunostaining of the lesion area. (A and B) Intense microglial activation (Ox42, red staining) was observed within lesion core surrounded by clear astroglial activation (GFAP, green staining). (C and D) NeuN immunostaining (red) was clearly decreased in lesion core when compared with surrounding healthy tissue.

also reported an increase in ^{11}C-PK11195 in various neuropathology (1.5- to ~2-fold increases in BP in Parkinson's disease, AD, stroke) (*13–16,28*). Overall, these observations validate our model of intrastriatal injection of AMPA in the rat, showing that microglia is strongly activated in the damaged brain area and that this lesion is associated with PBR expression, as shown by ^{3}H-PK11195 autoradiography. This result is in agreement with earlier reports showing PBR induction in other models of brain lesion (*12,16,18,29–32*). However, ^{11}C-PK11195 has a high nonspecific binding (26%–49% of total binding in our autoradiographic binding studies; data not shown), mainly due to high lipophicility and low bioavailability (88% of the ligand bound to plasma protein) (*18*). This has hampered the ability to easily quantify and model ^{11}C-PK11195 in vivo binding using PET and, although improvements in ^{11}C-PK11195 modeling have been recently published (*20*), the development of new PET radioligands with improved pharmacologic properties is eagerly awaited for more sensitive and more efficient PET of neuroinflammatory processes. Recently, several compounds (^{11}C-vinpocetine, ^{11}C-VC195, ^{11}C-DAA1106, ^{18}F-FMDAA1106, and ^{18}F-FEDAA1106) have been evaluated. Indeed, Maeda et al. (*33*), Zhang et al. (*34,35*), and Fujimara et al. (*36*) have extensively described ^{11}C-DAA1106 and

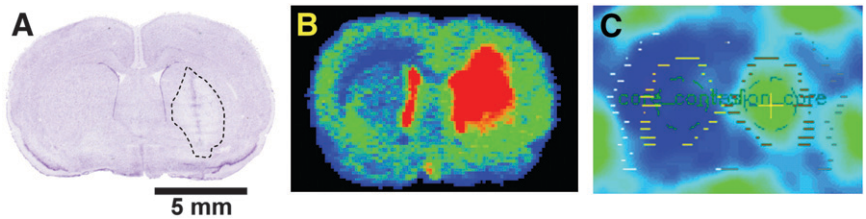

FIGURE 4. Cresyl violet–stained coronal section of a rat brain with lesion delineated by dashed area (A), ^{3}H-PK11195 autoradiographic image (B), and ^{11}C-PK11195 PET image (C).

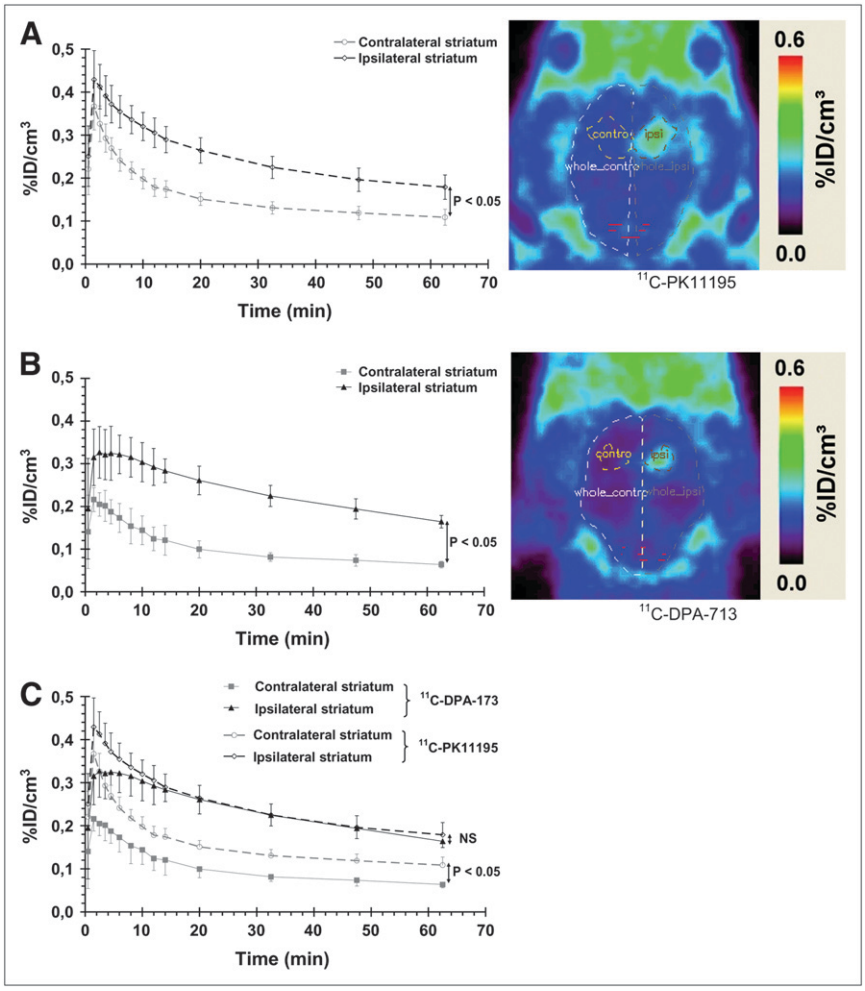

FIGURE 5. Time–activity curves for ^{11}C-PK11195 (n = 5) (A) and ^{11}C-DPA-713 (n = 4) (B) and corresponding quantitative PET images (right) and comparison between these 2 radioligands (C). Data are expressed as percentage of injected dose per cubic centimeter (%ID/cm^3; mean ± SD) as a function of postinjection time (min). Significant statistical differences are shown between ipsilateral and contralateral curves ($P <$ 0.05 from 2.5 min after injection for ^{11}C-PK11195 (A) and from 1.5 min after injection for ^{11}C-DPA-713 (B)) and between ^{11}C-PK11195 and ^{11}C-DPA-713 in the contralateral side (C) ($P < 0.05$, from 1.5 min after injection to end of measurement) (Mann–Whitney tests). Images shown at right are summed images between 2 and 70 min after injection. ipsi = ipsilateral; NS = not significant.

fluorinated derivatives in ex vivo binding experiments on rat brain sections and biodistribution in mice. They also performed PET on normal monkeys or healthy patients, but so far, to our knowledge, no published data from in vivo experiments combining DAA1106 and derivatives in brain with enhanced microglial activation have been published. Surprisingly, Maeda et al. (*33*) show relatively high uptake of DAA1106 and FEDAA1106 in the normal brain when compared with ^{11}C-PK11195, whereas PBR expression is supposed to remain very low in normal brain (*37*). They also report a total displacement of ^{11}C-DAA1106 by itself, but only a 50% displacement with 5 mg/kg of PK11195, which tends to support either (i) binding to another type of receptor or to different binding sites than PK11195 on the PBR (as suggested by the authors), (ii) nondisplaceable binding, or (iii) a higher nonspecific binding of ^{11}C-DAA1106 in vivo, which could be related to the higher lipophilicity of DAA1106 compared with PK11195 as mentioned by the authors. Guylas et al. (*38,39*) have investigated ^{11}C-vinpocetine using PET but only in healthy patients or monkeys, and pharmacologic data indicate that vinpocetine may bind to binding sites other than the PBR (*39*). Belloli et al. (*18*) have evaluated ^{11}C-labeled VC193M, VC195, and VC198M in a rat model of striatal lesion (quinolinic acid) and the in vivo distribution by microdissection of the brain. These authors have shown that VC195 depicted in vivo biodistribution and binding similar to PK11195 and, therefore, had the same potential as PK11195 as a PBR ligand. Overall, PET of these compounds needs to be compared with ^{11}C-PK11195, either in a relevant experimental model or in patients with a neuropathologic condition.

Here, we demonstrate that ^{11}C-DPA-713 exhibits a higher signal-to-noise ratio than ^{11}C-PK11195, likely because of a reduced uptake (likely to be related to nonspecific binding) in the healthy tissue when compared with ^{11}C-PK11195 (Fig. 5C). In the damaged tissue, expressing PBR, the time–activity curves are superimposable, although the pharmacokinetic of DPA-713 appears to be slower than that of PK11195 during the distribution phase (0–10 min). This latter point indicates that the difference observed could also be explained by a lower tracer delivery (K_1) for ^{11}C-DPA-713 than for ^{11}C-PK11195 in the tissue, likely to be due to a lower lipophilicity of ^{11}C-DPA-713 when compared with ^{11}C-PK11195 (log D: PK11195 = 3.35; DPA-713 = 2.41 (*22*)). If K_1 of ^{11}C-DPA-713 is lower, then the amount of available free ligand is reduced. Therefore,

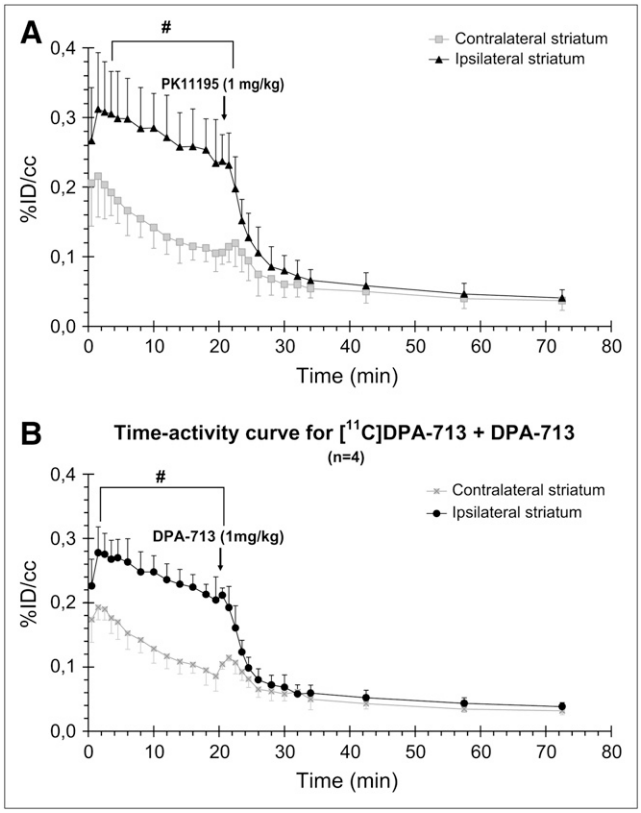

FIGURE 6. Time–activity curves for ^{11}C-DPA-713 displaced by excess of 1 mg/kg of either PK11195 (A) or DPA-713 (B) (n = 4 in each group) 20 min after injection of ^{11}C-DPA-713. Data are expressed as percentage of injected dose per cubic centimeter (%ID/cm^3; mean ± SD) as a function of postinjection time (min). #Significantly different from contralateral striatum ($P < 0.05$; Mann–Whitney test).

one might hypothesize that the reduction of signal seen in the contralateral ROI results from a lower free ligand concentration rather than from a lower nonspecific binding. If that is the case, with a lower amount of free ^{11}C-DPA-713 in the ipsilateral ROI and a nonspecific binding level similar for ^{11}C-DPA-713 and ^{11}C-PK11195, to observe a similar signal in the ipsilateral ROI, the specific binding of ^{11}C-DPA-713 has to be higher for ^{11}C-DPA-713 than that for ^{11}C-PK11195. This proposition assumes equal K_1 for both ROIs—that is, $k_1 = k'_1$ and $R_1 = 1$. To investigate the impact of the observed value of $R_1 = 1.32$ on the activity level in the ipsilateral ROI, we simulated a new PET curve for $R_1 = 1$, with k_2 and BP remaining the same, reflecting the conditions in which BBB would have remained intact at all times. The results show that, as early as 11 ± 3 min after injection, the simulated activity level is similar to our measurements and supports the notion that the BP calculated with the simplified reference tissue model reflects the true BP of ^{11}C-DPA-713.

Alternatively, the lower tracer delivery K_1 in the contralateral ROI could reflect a reduced DV_1 in that structure with respect to the ROI ipislateral to the lesion. However, it is highly unlikely that the DV_1 would vary between both structures, given the similarity of the ipsilateral and contralateral kinetics after injection of unlabeled ligand (Fig. 6).

The best way to clarify this question would be to measure the arterial plasma concentration during the PET experiment for both ligands and to estimate the parameters in all ROIs. Although our attempts to do so were not successful in this study, this question would need new investigations in larger animals, such as nonhuman primates, allowing easier arterial blood sampling to further investigate the modeling of ^{11}C-DPA-713.

DPA-713 is known to have an excellent specificity and affinity for PBR binding sites (*22,40*). Accordingly, after injection of an excess of either unlabeled PK11195 or DPA-713, our in vivo PET study showed (i) a short phase of slight signal increase expected from peripheral sites' release (*19*) (between 20 and 23 min), immediately followed by (ii) a full displacement of ^{11}C-DPA-713 (Fig. 6). Moreover, there was no displacement in the contralateral side, in correlation with the lack of activated microglia as shown by immunohistochemistry. This supports the use of the mirror ROI of the ipsilateral side as a reference compartment in the simplified reference tissue model used to model our PET data. Using this model, which assumes that no specific binding exists in the reference tissue (*27*), our data demonstrate a greater BP for ^{11}C-DPA-713 than that for ^{11}C-PK11195 and correlate with the better signal-to-noise ratio of ^{11}C-DPA-713.

CONCLUSION

In the present work, we report a combination of small-animal dedicated PET and the use of a model of neuroinflammation for a direct comparison of ^{11}C-PK11195 and the new PBR radioligand ^{11}C-DPA-713. Generally, our results (i) highlight the great interest in PET studies in small animals to screen and identify new radioligands directly in vivo, allowing a rapid translation to clinical PET, and (ii) open new perspectives for the investigation of neuroinflammatory processes in neuropathologic conditions and the follow-up of therapeutic interventions in animal models. More specifically, our results show that ^{11}C-DPA-713 has a greater potential for the quantification of PBR binding sites than ^{11}C-PK11195 because of its better signal-to-noise ratio. ^{11}C-DPA-713 is a very promising PBR radioligand, although further clinical studies are needed to validate the use of ^{11}C-DPA-713 in clinical imaging. An improved PBR PET radioligand, such as ^{11}C-DPA-713, is of great significance in the clinical studies of neurodegenerative diseases, where it would allow a more sensitive and accurate quantification of PBR induction, diffuse and of slight amplitude in neurodegenerative diseases or acute and precisely located in rather small ROIs in stroke or brain trauma. Such a radioligand will also dramatically enhance the ability to directly monitor neuroinflammatory processes (e.g., glial response) and to indirectly follow neuronal stress

induced by neuroinflammation. More capacity to measure these 2 parameters in patients would contribute to the development of reliable diagnostic and therapy follow-up tools.

ACKNOWLEDGMENTS

The authors thank Drs Bertrand Kuhnast and Sébastien Jan for their advice and input and Vincent Brulon, Yoann Fontyn, Benoit Jego, and Karine Siquier for their technical help. The authors also thank Prof. Silvia Selleri (Dipartimento di Scienze Farmaceutiche, Università di Firenze, Italy) for originally initiating studies on DPA compounds. This work was supported in part by a CEA/Sanofi-Aventis fellowship, by the European Molecular Imaging Laboratory network of excellence (LSH-2004-503569), and the CEA-CNRS "Imagerie du Petit Animal" program. This work was also supported by DEST and the French Embassy in Australia under the FAST program (FR040051).

REFERENCES

1. Bertram L, Tanzi RE. The genetic epidemiology of neurodegenerative disease. *J Clin Invest.* 2005;115:1449–1457.
2. Ferri CP, Prince M, Brayne C, et al. Global prevalence of dementia: a Delphi consensus study. *Lancet.* 2005;366:2112–2117.
3. Rothwell NJ. Neuroimmune interactions: the role of cytokines. *Br J Pharmacol.* 1997;121:841–847.
4. Nakajima K, Kohsaka S. Microglia: neuroprotective and neurotrophic cells in the central nervous system. *Curr Drug Targets Cardiovasc Haematol Disord.* 2004; 4:65–84.
5. Moran LB, Duke DC, Turkheimer FE, Banati RB, Graeber MB. Towards a transcriptome definition of microglial cells. *Neurogenetics.* 2004;5:95–108.
6. Yamashita K, Vogel P, Fritze K, Back T, Hossmann KA, Wiessner C. Monitoring the temporal and spatial activation pattern of astrocytes in focal cerebral ischemia using in situ hybridization to GFAP mRNA: comparison with sgp-2 and hsp70 mRNA and the effect of glutamate receptor antagonists. *Brain Res.* 1996; 735:285–297.
7. Rupalla K, Allegrini PR, Sauer D, Wiessner C. Time course of microglia activation and apoptosis in various brain regions after permanent focal cerebral ischemia in mice. *Acta Neuropathol (Berl).* 1998;96:172–178.
8. Pappata S, Levasseur M, Gunn RN, et al. Thalamic microglial activation in ischemic stroke detected in vivo by PET and [^{11}C]PK11195. *Neurology.* 2000;55: 1052–1054.
9. Ouchi Y, Yoshikawa E, Sekine Y, et al. Microglial activation and dopamine terminal loss in early Parkinson's disease. *Ann Neurol.* 2005;57:168–175.
10. Stephenson DT, Schober DA, Smalstig EB, Mincy RE, Gehlert DR, Clemens JA. Peripheral benzodiazepine receptors are colocalized with activated microglia following transient global forebrain ischemia in the rat. *J Neurosci.* 1995;15: 5263–5274.
11. Vowinckel E, Reutens D, Becher B, et al. PK11195 binding to the peripheral benzodiazepine receptor as a marker of microglia activation in multiple sclerosis and experimental autoimmune encephalomyelitis. *J Neurosci Res.* 1997;50:345–353.
12. Banati RB, Newcombe J, Gunn RN, et al. The peripheral benzodiazepine binding site in the brain in multiple sclerosis: quantitative in vivo imaging of microglia as a measure of disease activity. *Brain.* 2000;123:2321–2337.
13. Groom GN, Junck L, Foster NL, Frey KA, Kuhl DE. PET of peripheral benzodiazepine binding sites in the microgliosis of Alzheimer's disease. *J Nucl Med.* 1995;36:2207–2210.
14. Gerhard A, Pavese N, Hotton G et al. In vivo imaging of microglial activation with [11C](R)-PK11195 PET in idiopathic Parkinson's disease. *Neurobiol Dis.* 2005;21:404–412.
15. Turner MR, Cagnin A, Turkheimer FE, et al. Evidence of widespread cerebral microglial activation in amyotrophic lateral sclerosis: an [^{11}C](R)-PK11195 positron emission tomography study. *Neurobiol Dis.* 2004;15:601–609.
16. Cagnin A, Brooks DJ, Kennedy AM, et al. In-vivo measurement of activated microglia in dementia. *Lancet.* 2001;358:461–467.
17. Benavides J, Quarteronet D, Imbault F, et al. Labelling of "peripheral-type" benzodiazepine binding sites in the rat brain by using [^{3}H]PK 11195, an isoquinoline carboxamide derivative: kinetic studies and autoradiographic localization. *J Neurochem.* 1983;41:1744–1750.
18. Belloli S, Moresco RM, Matarrese M, et al. Evaluation of three quinoline-carboxamide derivatives as potential radioligands for the in vivo PET imaging of neurodegeneration. *Neurochem Int.* 2004;44:433–440.
19. Petit-Taboue MC, Baron JC, Barre L, et al. Brain kinetics and specific binding of [^{11}C]PK 11195 to omega 3 sites in baboons: positron emission tomography study. *Eur J Pharmacol.* 1991;200:347–351.
20. Kropholler MA, Boellaard R, Schuitemaker A, et al. Development of a tracer kinetic plasma input model for (R)-[^{11}C]PK11195 brain studies. *J Cereb Blood Flow Metab.* 2005;25:842–851.
21. Lockhart A, Davis B, Matthews JC, et al. The peripheral benzodiazepine receptor ligand PK11195 binds with high affinity to the acute phase reactant alpha1-acid glycoprotein: implications for the use of the ligand as a CNS inflammatory marker. *Nucl Med Biol.* 2003;30:199–206.
22. James ML, Fulton RR, Henderson DJ, et al. Synthesis and in vivo evaluation of a novel peripheral benzodiazepine receptor PET radioligand. *Bioorg Med Chem.* 2005;13:6188–6194.
23. Thominiaux C, Dolle F, James ML, et al. Improved synthesis of the peripheral benzodiazepine receptor ligand [^{11}C]DPA-713 using [^{11}C]methyl triflate. *Appl Radiat Isot.* 2006;64:570–573.
24. Osborne KA, Shigeno T, Balarsky A-M, et al. Quantitative assessment of early brain damage in a rat model of focal cerebral ischemia. *J Neurol Neurosurg Psychol.* 1987;50:402–410.
25. Camsonne R, Crouzel C, Comar D, et al. Synthesis of N-(11-C) methyl, N-(methyl-1 propyl), (chloro-2 phenyl)-1 isoquinoleine carboxamide-3 (PK 11195): a new ligand for peripheral benzodiazepine receptors. *J Labelled Compds Radiopharm.* 1984;21:985–991.
26. Cremer JE, Hume SP, Cullen BM, et al. The distribution of radioactivity in brains of rats given [N-methyl-^{11}C]PK 11195 in vivo after induction of a cortical ischaemic lesion. *Int J Rad Appl Instrum B.* 1992;19:159–166.
27. Lammertsma AA, Hume SP. Simplified reference tissue model for PET receptor studies. *Neuroimage.* 1996;4:153–158.
28. Price CJ, Wang D, Menon DK, et al. Intrinsic activated microglia map to the peri-infarct zone in the subacute phase of ischemic stroke. *Stroke.* 2006;37:1749–1753.
29. Sette G, Baron JC, Young AR, et al. *In vivo* mapping of brain benzodiazepine receptor changes by positron emission tomography after focal ischemia in the anesthetized baboon. *Stroke.* 1993;24:2046–2057.
30. Rao VL, Bowen KK, Rao AM, Dempsey RJ. Up-regulation of the peripheral-type benzodiazepine receptor expression and [^{3}H]PK11195 binding in gerbil hippocampus after transient forebrain ischemia. *J Neurosci Res.* 2001;64:493–500.
31. Biegon A, Alvarado M, Budinger TF, et al. Region-selective effects of neuroinflammation and antioxidant treatment on peripheral benzodiazepine receptors and NMDA receptors in the rat brain. *J Neurochem.* 2002;82:924–934.
32. Ryu JK, Choi HB, McLarnon JG. Peripheral benzodiazepine receptor ligand PK11195 reduces microglial activation and neuronal death in quinolinic acid-injected rat striatum. *Neurobiol Dis.* 2005;20:550–561.
33. Maeda J, Suhara T, Zhang MR, et al. Novel peripheral benzodiazepine receptor ligand [^{11}C]DAA1106 for PET: an imaging tool for glial cells in the brain. *Synapse.* 2004;52:283–291.
34. Zhang MR, Kida T, Noguchi J, et al. [^{11}C]DAA1106: radiosynthesis and in vivo binding to peripheral benzodiazepine receptors in mouse brain. *Nucl Med Biol.* 2003;30:513–519.
35. Zhang MR, Maeda J, Ogawa M, et al. Development of a new radioligand, N-(5-fluoro-2-phenoxyphenyl)-N-(2-[^{18}F]fluoroethyl-5-methoxybenzyl)acetamide, for PET imaging of peripheral benzodiazepine receptor in primate brain. *J Med Chem.* 2004;47:2228–2235.
36. Fujimura Y, Ikoma Y, Yasuno F, et al. Quantitative analyses of ^{18}F-FEDAA1106 binding to peripheral benzodiazepine receptors in living human brain. *J Nucl Med.* 2006;47:43–50.
37. Benavides J, Guilloux F, Rufat P, et al. In vivo labelling in several rat tissues of 'peripheral type' benzodiazepine binding sites. *Eur J Pharmacol.* 1984;99:1–7.
38. Gulyas B, Halldin C, Vas A, et al. [^{11}C]Vinpocetine: a prospective peripheral benzodiazepine receptor ligand for primate PET studies. *J Neurol Sci.* 2005;229–230:219–223.
39. Gulyas B, Halldin C, Sandell J, et al. PET studies on the brain uptake and regional distribution of [^{11}C]vinpocetine in human subjects. *Acta Neurol Scand.* 2002;106:325–332.
40. Selleri S, Bruni F, Costagli C, et al. 2-Arylpyrazolo[1,5-a]pyrimidin-3-yl acetamides: new potent and selective peripheral benzodiazepine receptor ligands. *Bioorg Med Chem.* 2001;9:2661–2671.